Time-lapse Ground Penetrating Radar Full-waveform Inversion to detect tracer plumes, a numerical study

Peleg Haruzi [a,*], *Nils Gueting* [a], *Anja Klotzsche* [a,b], *Jan Vanderborght* [a,b], *Harry Vereecken* [a,b], *Jan van der Kruk* [a,b]
[a]*Agrosphere Institute, IBG-3, Forschungszentrum Jülich GmbH*
[b]*Centre for High-Performance Scientific Computing in Terrestrial Systems (HPSC-TerrSys), Geoverbund ABC/J*

Summary

Time-lapse geophysical imaging of tracer tests is essential to infer channelized transport properties. Cross-hole ground-penetrating radar (GPR) tomography is a high resolution imaging method to characterize the near-surface. We present preliminary results of crosshole GPR full-waveform inversion of time-lapse synthetic data during a saline tracer test. The tracer movement was obtained from a 3D transport simulation in a hydrogeological model representing the Krauthausen aquifer where in future also field tests will be performed. The full-waveform inversion accurately resolved the infiltrated tracer distribution in the plane within decimeter scale. The results indicate the potential of GPR full-waveform inversion for saline tracer detection and high-resolution time-lapse transport characterization.

Introduction

Time-lapse geophysical imaging methods are used in environmental science and engineering to monitor tracer migration (Singha and Gorelick, 2005), contaminant leaks (Binley et al., 1997), tide-driven salinity changes (Slater and Sandberg, 2000), hydrogeophysical characterization of transport processes (Shakas et al., 2016) and other applications. Time-lapse changes can be quantitatively characterized due to the changing geophysical properties of the groundwater and soil states. Especially, GPR has shown a high potential to map and monitor time-lapse changes. The method is able to provide two electromagnetic properties the relative permittivity ε_r and electrical conductivity σ_b, while both parameters are sensitive to soil water content, salinity and soil texture. Until now, permittivity measurements were used to monitor water content changes using GPR (Daily and Ramirez, 1989; Huisman et al., 2003), and electrical conductivity to indicate changes in salinity using ERT studies (Daily et al. 1992; Müller et al. 2010) and changes in temperature (Ramirez et al., 1993; Hermans et al., 2005). Time-lapse numerical simulations to evaluate the potential of geophysical imaging techniques have been used to investigate GPR mapping of DNAPL-spill (Wilson et al., 2009) and ERT inferring aquifer transport characteristics (Vanderborght et al., 2005).

Cross-hole ground-penetrating radar (GPR) tomography is a powerful tool to map the spatial distribution of subsurface properties such as porosity (Nielsen et al., 2010), moisture content (Binley et al., 2001), and flow and transport properties (Day-Lewis et al., 2003). Models for permittivity and conductivity are often achieved by ray-based inversion techniques which use first arrival travel times and first cycle amplitudes of the measured signal. However, inversion models of these methods are smoothed and have low-resolution. Improved resolution is obtained using the full waveform inversion (FWI) method where the entire received signal is used in the inversion technique (Ernst et al., 2007a). GPR-FWI was tested on synthetic crosshole data (Ernst et al., 2007b, Meles et al., 2010) and was proven successful in characterizing a gravel aquifer (e.g. Klotzsche et al., 2010) and for porosity estimation in chalk (Keskinen et al., 2017).
In this work, synthetic time-lapse GPR-FWI imaging of a saline tracer test was performed to test the potential of GPR-FWI to detect transport processes in a hydrogeological model of an alluvial aquifer. Thereby, testing different synthetic tracer scenarios will allow us to better predict and plan an optimized field tracer test.

3D hydrogeological model of the Krauthausen aquifer

The Krauthausen test site in Germany has been investigated by well logging, time-lapse tracer measurements (Vereecken et al., 2000; Kemna et al., 2002), cone penetration tests (Tillmann et al., 2008), direct-push hydraulics measurements (Gueting et al., 2017), and high-resolution GPR-FWI (Gueting et al., 2015). These investigations allowed to derive the spatial variability of the basic aquifer parameters, transport properties, hydraulic conductivity and porosity. As a first stage of the 3D model created by Gueting et al. (2018), co-located data of GPR and grain size along 3 boreholes were used to derive an empirical relationship between GPR properties and grain size (Gueting et al., 2017). This relationship was used to predict the distribution of three grain size facies at locations where no grain size data exist. From 2D GPR planes (white dashed lines in Figure 1), a 3D hydrogeological model was constructed using multiple-point statistics simulation (Gueting et al., 2018).

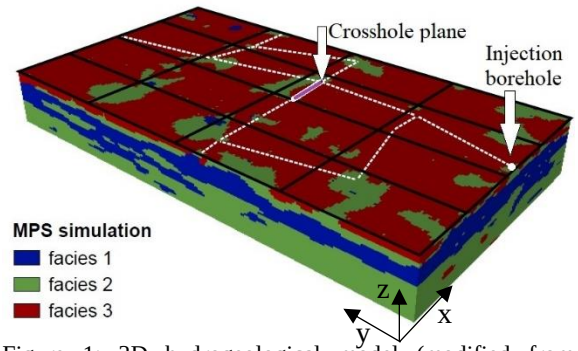

Figure 1: 3D hydrogeological model (modified from Gueting et al. (2018). White dot and purple line show the locations in the numerical test of the injection borehole and the GPR crosshole plane, respectively. The model dimensions are $23\text{x}44\text{x}5.4\ m^3$ and the cell size is $(0.18m)^3$.

Facie	$K[m/day]$	ϕ	$\alpha_L[m]$	$\alpha_T[m]$
1 (sand)	14.3	0.29	0.1	0.01
2 (sandy gravel)	70.2	0.25	0.1	0.01
3 (gravel)	626	0.18	0.1	0.01

Table 1: Flow and transport parameters of the 3D model: hydraulic conductivity (K), porosity (ϕ), longitudinal (α_L) and transverse dispersivity (α_T).

Tracer transport simulation

Flow and transport simulations were used to predict the tracer distribution in time and space in the 3D Krauthausen model. Hydraulic and transport parameters related to the Krauthausen aquifer were adapted from Gueting et al. (2017) and Vanderborght et al. (2005) as shown in Table 1. A natural hydraulic gradient of -0.002 (from Müller et al., 2010) is applied between the xz planes of the model to stimulate flow along the y-axis. Given the velocity field from the flow simulation, transport of a conservative halite (NaCl) solute injected through a whole column of a borehole (see injection borehole in Figure 1) in the saturated porous medium is modelled and governed by the advection-dispersion equation (ADE). The flow and transport simulations were computed by the TRACE and PARTRACE codes using the particle tracking method (Vereecken et al., 1994 and Neuendorf et al., 1997). The result of the transport simulation is a spatio-temporal distribution of tracer concentration.

Petrophysical relations

In order to monitor the tracer distribution with ground penetrating radar, petrophysical relations are required to convert the tracer concentration to bulk relative permittivity (ε_r) and electrical conductivity (σ_b). Whereas permittivity is not affected by introducing electrolytes in the groundwater, bulk conductivity is influenced by it (Giannakis, 2016). First, the total groundwater salinity $S_{GW,Total}$ was calculated as sum of the ambient salinity and the tracer salinity:

$$S_{GW,Total}(\boldsymbol{x},t) = S_{GW,ambient} + \frac{C(\boldsymbol{x},t)}{C_{injection}} \times S_{injection}. \quad (1)$$

where $C(\boldsymbol{x},t)$ is the spatio-temporal tracer concentration, and $C_{injection}$ and $S_{injection}$ are the injected tracer concentration and salinity. Then, the water conductivity was related to salinity and temperature of the water using empirical relations (Stogryn, 1971):

$$\sigma_{GW}(\boldsymbol{x},t) = f(S_{GW}(\boldsymbol{x},t),T). \quad (2)$$

Finally, the bulk conductivity was calculated from Archie's empirical law (Archie, 1942):

$$\sigma_b(\boldsymbol{x},t) = \frac{\sigma_{GW}(\boldsymbol{x},t)}{F(\boldsymbol{x})}, \quad (3)$$

where the electrical formation factor F is an intrinsic measure of material microgeometry. $F(\boldsymbol{x})$ was calculated once in *ambient* conditions from GPR-FWI bulk conductivity $\sigma_b(\boldsymbol{x})$ (Figure 2b) and measured uniform groundwater conductivity σ_{GW}, using Equation 3.

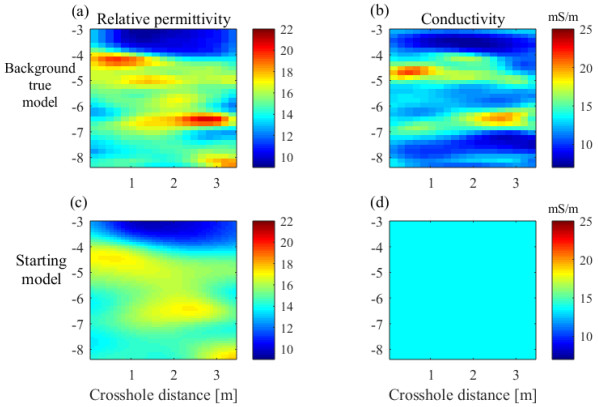

Figure 2: Relative permittivity and conductivity background true models (a, b) and starting models (c, d) for the FWI.

GPR synthetic and Full Waveform inversion

At selected times during the tracer test, synthetic crosshole GPR forward model simulations were performed in a plane perpendicular to the mean flow direction located 20 m downstream from the injection borehole (Figure 1). The synthetic crosshole GPR datasets were calculated using a Ricker wavelet with 120 MHz centre frequency. Multi-offset gather (MOG) data using a semi-reciprocal acquisition setup with spatial sampling of 0.1 m and 0.2 m for the receivers and transmitters, respectively, were calculated to obtain a high resolution of the full-waveform inversion (Oberröhrmann et al., 2013). The MOG dataset consists of 56 gathers and each gather has 55 traces.

The full-waveform tomographic inversion scheme (Meles et al., 2010) returned spatial distributions of ε_r and σ_b that minimize the squared norm $S(\varepsilon_r, \sigma_b)$ of the difference between the FWI inverted model data and the observed data that resulted from the forward model simulations by using the "true model"). Crosshole planes during the tracer

infiltration are inverted by FWI, and models are compared to the background FWI model to calculate the differences in permittivity and conductivity. The background true model (Figures 2a, b) which is used in a forward model to calculate the observed data is taken from a GPR-FWI plane as estimated by Gueting et al., 2017. The permittivity true model (Figure 2a) is the same for all scenarios for the reason given in the former subsection. For both the background and tracer scenarios, the permittivity starting model for the FWI is a smoothed image of the background (Figure 2c) and for the conductivity (Figure 2d) starting model is a uniform average value of the background conductivity, $\sigma_b = 13.3\ \mathrm{mS/m}$.

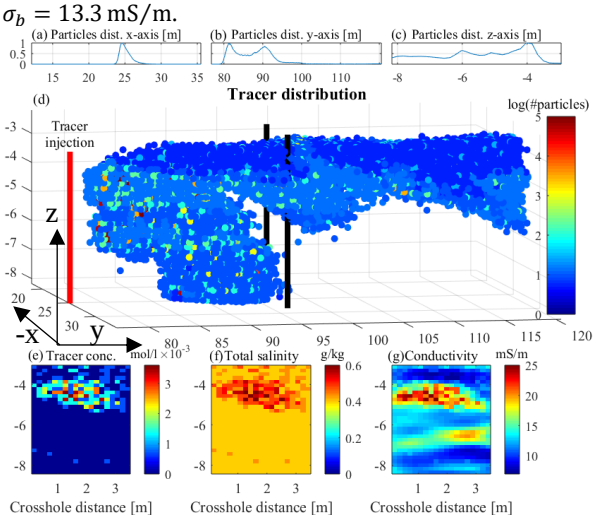

Figure 3: 3D transport simulation 20 days after injection (a-c) spatial distribution of the tracer in planes across x-,y-z-axes. (d) 3D spatial distribution of the particles. (e-g) tracer concentration, total groundwater salinity and electrical conductivity in a plane perpendicular to the mean flow velocity (between the black columns in (d)).

Results and Discussion

Results of the 3D transport simulation 20 days after the injection are shown in Figure 3. Time-lapse observation reveals that a part of the tracer plume is transported quickly at depths between 3-3.5m (Figure 3d). This depth belongs to the gravel facie 3, showing a narrow hydraulically conductive layer (Figure 1, Table 1). A slower and larger part of the tracer plume travels at the bottom of the model between depths 6.3-8.25 m in a thicker and less conductive sandy gravel facie 2. Vertical transverse dispersion of particles belonging to the upper part of the plume causes a continuous decrease in tracer particles at 3-3.5 m depths (Figure 3c) and an increase at a depth of ~4m in facies 1 and 2 with higher porosity. At depths between 6.3-8.25 m we observe a lower transverse dispersion than at the top layer because of lower velocity. Along the x-axis the spreading behaviour of the plume is almost Gaussian (Figure 3a) due to transverse dispersion. The horizontal layering in the 3D model generated a larger horizontal surface area of the plume front in the horizontal orientation, which led a larger transverse dispersion in the direction of the z-axis than in direction of the x-axis.

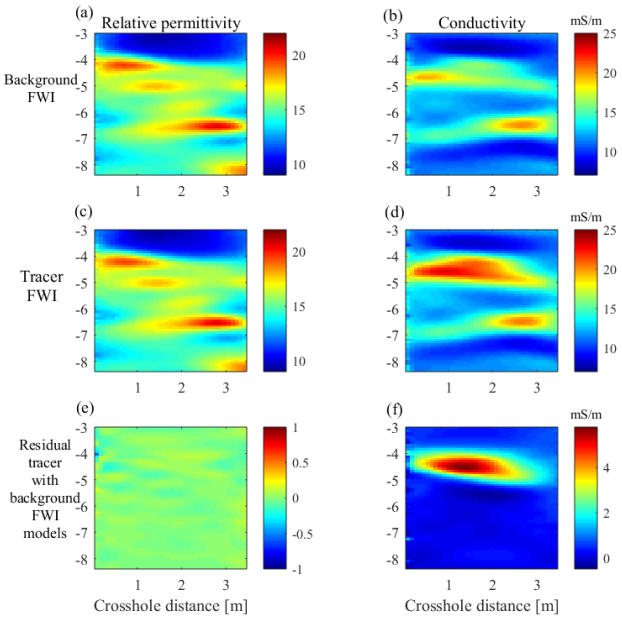

Figure 4: (a, b) FWI results of background model; (c, d) FWI results of tracer model data 20 days after injection; (e) Difference of permittivity models (c) and (a); (f) Difference of conductivity models (d) and (b).

Synthetic GPR Full-waveform inversion

Twenty days after the injection the tracer passes the crosshole plane at 4-5.5 m depths. At that time the plume width is about 3m (Figure 3e). We converted concentrations into salinity and then to conductivity (Figures 3f, g) using Equations 1-3 (groundwater ambient salinity was calculated to 0.398 g/kg). Injection of 20% seawater salinity (7.1 g/kg) was used to test the GPR-FWI, where after 20m transport distance the maximal total salinity was 0.64 g/kg, corresponding to a maximal bulk conductivity of 26 mS/m. The conductivity plane in Figure 3g is the true model used for the forward model to obtain the "observed" data that will be inverted with the FWI approach to investigate the reconstruction possibilities.

The FWI results for the background and tracer models are shown in Figures 4a-d. The background model was successfully reconstructed and returned very similar images compared to the true model (compare Figures 4a, b with 2a, b). Also the FWI of the tracer data is in agreement with the true model (compare Figures 4c and 2a). As expected, the tracer and background FWI permittivity models are very similar and show a low residual (Figure 4e). The difference between the FWI conductivity models of the tracer and background data resulted in a smoothed reconstruction of the plume (compare Figures 3f and 4f) having a maximal bulk conductivity of 5.79 mS/m. The average tracer salinity

at the centre of the plume obtained from FWI (0.16 g/kg) is similar to that from the transport simulation (0.12 g/kg).

In addition to the residual of FWI model planes to test the inversion, we compared the transmitter gathers (see Keskinen et al., 2017) of the observed and modelled data based on the FWI results (Figure 5b, c) and investigate the residual (Figure 5d). The residual is very small, suggesting that the FWI converged successfully to the observed data. Comparison between the background modelled data (Figure 5a) and tracer modelled data shows large differences in amplitudes for transmitter gathers located at the upper part of the boreholes (traces 200-800 for transmitters at the left borehole, and traces 1700-2300 at the right borehole). This amplitude difference is explained by the conductivity and thus attenuating tracer plume that infiltrated in the upper part of the measured plane, which is in agreement with the residual in permittivity and conductivity FWI model planes (Figure 4e, f).

Note that the occurrence of the tracer at depths shallower than 4.75m through the crosshole plane was not detected in a time-lapse ERT tracer test in Krauthausen (Müller et al., 2010). Close observation shows that the upper part of the model near the injection borehole (white dot in Figure 1) is located in facie 2 having a lower conductivity than facie 3. We suggest that the upper part of the injection borehole (~3-4.75m depths) has even lower conductivity or is clogged, thus constraining the tracer from traveling through the aquifer at shallow depths.

For future work, we plan to test the full-waveform inversion with larger conductivity contrasts in synthetic tests. Based on the prediction from transport simulations and the ability of synthetic GPR-FWI to detect the tracer in various concentrations, a field tracer test will be planned.

Acknowledgements

This study is part the Enigma ITN program (European training Network for in situ imaGing of dynaMic processes in heterogeneous subsurfAce environments). This project has received funding from the European Union's Horizon 2020 research and innovation programme under the Marie Sklodowska-Curie Grant Agreement No 722028.

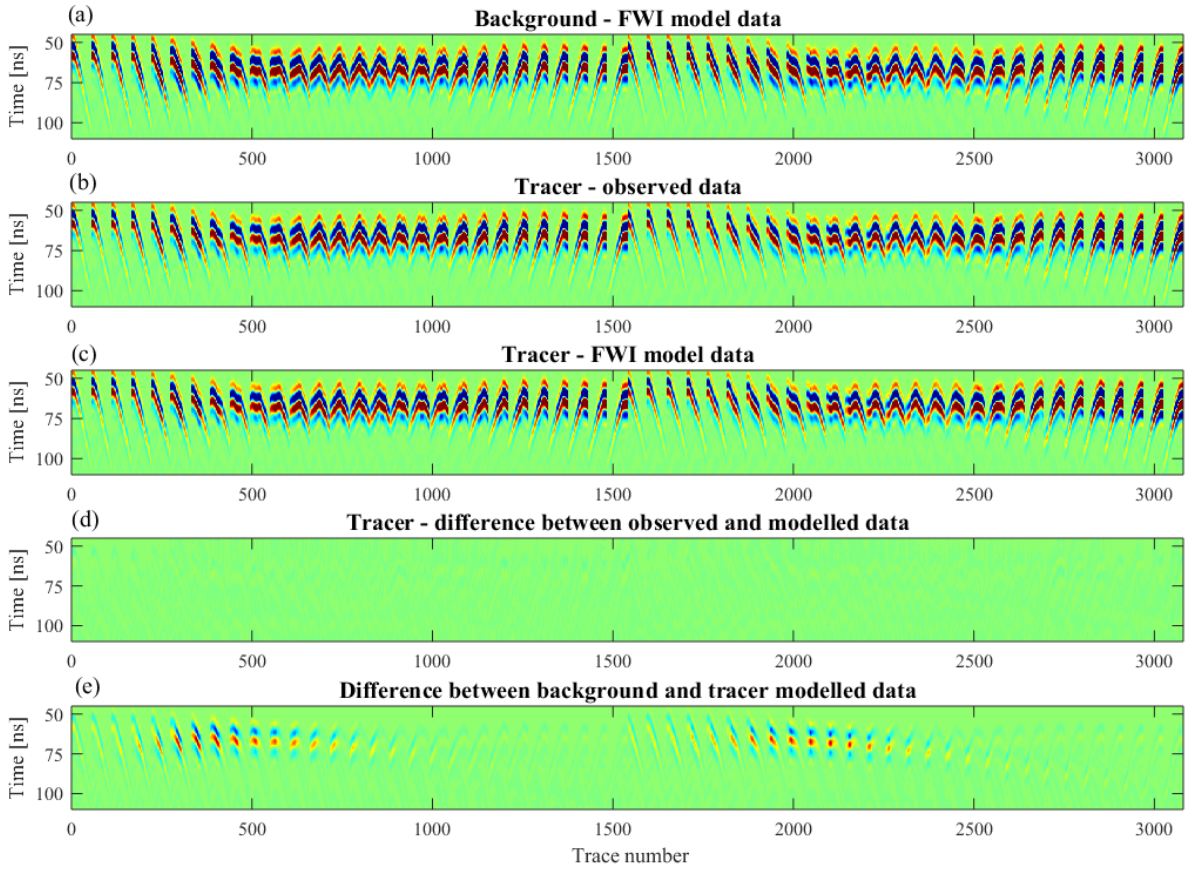

Figure 5: (a) Background FWI modelled data. (b) Tracer observed data. (c) Tracer FWI modelled data. (d) Residual of the tracer modelled data obtained from the FWI results with the observed data. (e) Difference between tracer FWI modelled data with the background FWI modelled data. The x-axis denotes trace number starting from the first trace of first transmitter gather and ending to last trace of last transmitter gather.

References

Archie, G. E. (1942). The electrical resistivity log as an aid in determining some reservoir characteristics. Transactions of the AIME, 146(01), 54-62.

Binley, A., Daily, W., & Ramirez, A. (1997). Detecting leaks from environmental barriers using electrical current imaging. Journal of Environmental and Engineering Geophysics, 2(1), 11-19.

Binley, A., Winship, P., Middleton, R., Pokar, M., & West, J. (2001). High-resolution characterization of vadose zone dynamics using cross-borehole radar. Water Resources Research, 37(11), 2639-2652.

Daily, W., & Ramirez, A. (1989). Evaluation of electromagnetic tomography to map in situ water in heated welded tuff. Water Resources Research, 25(6), 1083-1096.

Daily, W., Ramirez, A., LaBrecque, D., & Nitao, J. (1992). Electrical resistivity tomography of vadose water movement. Water Resources Research, 28(5), 1429-1442.

Ernst, J. R., Green, A. G., Maurer, H., & Holliger, K. (2007b). Application of a new 2D time-domain full-waveform inversion scheme to crosshole radar data. Geophysics, 72(5), J53-J64.

Ernst, J. R., Maurer, H., Green, A. G., & Holliger, K. (2007a). Full-waveform inversion of crosshole radar data based on 2-D finite-difference time-domain solutions of Maxwell's equations. IEEE transactions on geoscience and remote sensing, 45(9), 2807-2828.

Giannakis, I. (2016). Realistic numerical modelling of ground penetrating radar for landmine detection.

Gueting, N., Caers, J., Comunian, A., Vanderborght, J., & Englert, A. (2018). Reconstruction of Three-Dimensional Aquifer Heterogeneity from Two-Dimensional Geophysical Data. Mathematical Geosciences, 1-23.

Gueting, N., Klotzsche, A., van der Kruk, J., Vanderborght, J., Vereecken, H., & Englert, A. (2015). Imaging and characterization of facies heterogeneity in an alluvial aquifer using GPR full-waveform inversion and cone penetration tests. Journal of hydrology, 524, 680-695.

Gueting, N., Vienken, T., Klotzsche, A., van der Kruk, J., Vanderborght, J., Caers, J., ... & Englert, A. (2017). High resolution aquifer characterization using crosshole GPR full-waveform tomography: Comparison with direct-push and tracer test data. Water Resources Research, 53(1), 49-72.

Hermans, T., Wildemeersch, S., Jamin, P., Orban, P., Brouyère, S., Dassargues, A., & Nguyen, F. (2015). Quantitative temperature monitoring of a heat tracing experiment using cross-borehole ERT. Geothermics, 53, 14-26.

Huisman, J. A., Hubbard, S. S., Redman, J. D., & Annan, A. P. (2003). Measuring soil water content with ground penetrating radar. Vadose zone journal, 2(4), 476-491.

Kemna, A., Vanderborght, J., Kulessa, B., & Vereecken, H. (2002). Imaging and characterisation of subsurface solute transport using electrical resistivity tomography (ERT) and equivalent transport models. Journal of Hydrology, 267(3-4), 125-146.

Keskinen, J., Klotzsche, A., Looms, M. C., Moreau, J., van der Kruk, J., Holliger, K., ... & Nielsen, L. (2017). Full-waveform inversion of Crosshole GPR data: Implications for porosity estimation in chalk. Journal of Applied Geophysics, 140, 102-116.

Klotzsche, A., van der Kruk, J., Meles, G. A., Doetsch, J., Maurer, H., & Linde, N. (2010). Full-waveform inversion of cross-hole ground-penetrating radar data to characterize a gravel aquifer close to the Thur River, Switzerland. Near surface geophysics, 8(6), 635-649.

Meles, G. A., Van der Kruk, J., Greenhalgh, S. A., Ernst, J. R., Maurer, H., & Green, A. G. (2010). A new vector waveform inversion algorithm for simultaneous updating of conductivity and permittivity parameters from combination crosshole/borehole-to-surface GPR data. IEEE Transactions on geoscience and remote sensing, 48(9), 3391-3407.

Müller, K., Vanderborght, J., Englert, A., Kemna, A., Huisman, J. A., Rings, J., & Vereecken, H. (2010). Imaging and characterization of solute transport during two tracer tests in a shallow aquifer using electrical resistivity tomography and multilevel groundwater samplers. Water Resources Research, 46(3).

Neuendorf, O. (1997), Numerische 3D-Simulation des Stofftransports in einem heterogenen Aquifer, report, Forschungszentrum Jülich GmbH, Jülich, Germany.

Nielsen, L., Looms, M. C., Hansen, T. M., Cordua, K. S., & Stemmerik, L. (2010). Estimation of chalk heterogeneity from stochastic modelling conditioned by crosshole GPR travel times and LOG data: in R. Advances in near-surface seismology and ground-penetrating radar: SEG Geophysical Development Series, 15, 379-398.

Oberroehrmann, M., Klotzsche, A., Vereecken, H., & van der Kruk, J. (2013). Optimization of acquisition setup for cross-hole GPR full-waveform inversion using checkerboard analysis. Near Surface Geophysics, 11(2), 197-209.

Ramirez, A., Daily, W., LaBrecque, D., Owen, E., & Chesnut, D. (1993). Monitoring an underground steam injection process using electrical resistance tomography. Water Resources Research, 29(1), 73-87.

Shakas, A., Linde, N., Baron, L., Bochet, O., Bour, O., & Le Borgne, T. (2016). Hydrogeophysical characterization of transport processes in fractured rock by combining push-pull and single-hole ground penetrating radar experiments. Water Resources Research, 52(2), 938-953.

Singha, K., & Gorelick, S. M. (2005). Saline tracer visualized with three-dimensional electrical resistivity tomography: Field-scale spatial moment analysis. Water Resources Research, 41(5).

Slater, L. D., & Sandberg, S. K. (2000). Resistivity and induced polarization monitoring of salt transport under natural hydraulic gradients. Geophysics, 65(2), 408-420.

Stogryn, A. (1971). Equations for calculating the dielectric constant of saline water (correspondence). IEEE transactions on microwave theory and Techniques, 19(8), 733-736.

Tillmann, A., Englert, A., Nyári, Z., Fejes, I., Vanderborght, J., & Vereecken, H. (2008). Characterization of subsoil heterogeneity, estimation of grain size distribution and hydraulic conductivity at the Krauthausen test site using cone penetration test. Journal of contaminant hydrology, 95(1-2), 57-75.

Vanderborght, J., Kemna, A., Hardelauf, H., & Vereecken, H. (2005). Potential of electrical resistivity tomography to infer aquifer transport characteristics from tracer studies: A synthetic case study. Water Resources Research, 41(6).

Vereecken, H., Döring, U., Hardelauf, H., Jaekel, U., Hashagen, U., Neuendorf, O., ... & Seidemann, R. (2000). Analysis of solute transport in a heterogeneous aquifer: the Krauthausen field experiment. Journal of Contaminant Hydrology, 45(3-4), 329-358.

Vereecken, H.,G. Lindenmayr,O. Neuenedorf, U. Döring, and R. Seidemann (1994), TRACE: A mathematical model for reactive transport in 3D variable saturated porous media, ICG-4 Int. Rep. 501494, Forschungszentrum Jülich GmbH, Jülich, Germany.

Wilson, V., Power, C., Giannopoulos, A., Gerhard, J., & Grant, G. (2009). DNAPL mapping by ground penetrating radar examined via numerical simulation. Journal of Applied Geophysics, 69(3-4), 140-149.